

# Thesis Title

*A subtitle of your thesis*

Author name



Thesis submitted for the degree of  
Master in Master's Program Name <change at  
main.tex>  
60 credits

Department Name <change at main.tex>  
Faculty name <change in duoforside.tex>

UNIVERSITY OF OSLO

Spring 2022



# Thesis Title

*A subtitle of your thesis*

Author name

© 2022 Author name

Thesis Title

<http://www.duo.uio.no/>

Printed: Reprosentralen, University of Oslo

# **Abstract**

# Contents

<b>1</b>	<b>Introduction</b>	<b>1</b>
<b>I</b>	<b>Theory</b>	<b>3</b>
<b>2</b>	<b>Background</b>	<b>4</b>
2.1	Overview of sold-state physics . . . . .	4
2.2	3d Silicides . . . . .	4
<b>3</b>	<b>High-Entropy alloys</b>	<b>5</b>
3.1	Fundamentals . . . . .	5
3.2	Core effects and properties of high-entropy alloys . . . . .	8
<b>4</b>	<b>Special quasi-random Structures</b>	<b>10</b>
4.1	The concept and fundamentals of SQS - Write proper later . . . . .	10
4.2	Mathematical formulation: Might need to expand on the definition and meaning behind terms such as clusters, figures, correlation functions etc (Add in post!) . . . . .	11
4.3	Results and Advances in SQS and application to high-entropy alloys . . . . .	14
<b>5</b>	<b>Density-Functional Theory</b>	<b>15</b>
5.1	Review of Quantum Mechanics . . . . .	15
5.1.1	The Shrödinger equation . . . . .	15
5.1.2	Simplifications and approximations to solve the many-electron Shrödinger equation . . . . .	16
5.2	Fundamentals of Density-Functional Theory . . . . .	17
5.3	The exchange-correlation energy . . . . .	18
5.4	Success and limitation of DFT . . . . .	20
<b>II</b>	<b>Methodology and Implementation</b>	<b>21</b>
<b>6</b>	<b>Practical application of DFT</b>	<b>22</b>
<b>7</b>	<b>Computational details</b>	<b>25</b>
7.1	Vienna Ab initio Simulation Package . . . . .	25
7.2	Generation of SQS . . . . .	27

7.3	Utility scripts . . . . .	27
<b>III</b>	<b>Results and Discussion</b>	<b>28</b>
<b>8</b>	<b>Results of SQS</b>	<b>29</b>
8.1	Something . . . . .	29
<b>9</b>	<b>Band gap results</b>	<b>30</b>
9.1	Compare and anlayze band gaps . . . . .	30
<b>IV</b>	<b>Conclusion</b>	<b>31</b>

# List of Figures

3.1	Formation of HEA based on $\delta$ and $N$ . Figures adopted from [1] . . . . .	7
3.2	A schematic illustration of lattice distortion in high-entropy alloys. Figure from [2] . . . . .	9



# List of Tables

# Preface

# Chapter 1

## Introduction

some introduction on the importance of discovering new materials and alloying.

High-entropy alloys is a novel class of materials based on alloying multiple components, as opposed to the more traditional binary alloys. This results in an unprecedented opportunity for discovery of new materials with a superior degree of tuning for specific properties and applications. Recent research on high-entropy alloys have resulted in materials with exceedingly strong mechanical properties such as strength, corrosion and temperature resistance, etc **find references**. Meanwhile, the functional properties of high-entropy alloys is vastly unexplored. In this study, we attempt to broaden the knowledge of this field, the precise formulation of this thesis would be an exploration on the possibilities of semiconducting high-entropy alloys.

A key motivation of this thesis is the ability to perform such a broad study of complex materials in light of the advances in material informatics and computational methods. In this project, we will employ Ab initio methods backed by density functional theory on top-of the line supercomputers and software. 20 years ago, at the breaking point of these methods, this study would have been significantly narrower and less detailed firstly, but secondly would have totaled ... amount of CPU hours to complete (**Calculate this number**). In the addition to the development in computational power, is also the progress of modeling materials, specifically we will apply a method called Special Quasi-random Structures (SQS) to model high-entropy alloys or generally computationally complex structures. Together with the open landscape of high-entropy alloys described above, these factors produce a relevant study in the direction of applying modern computational methods to progress the research of a novel material class and indicate promising directions within the field.

In specifics, this thesis revolve around the electrical properties of high-entropy alloys, mainly the band gap as this is the key indicator for a semiconducting material and it's applicability. Semiconductors are the building blocks in many different applications in today's world, ranging from optical and electrical devices, to renewable energy sources such as

solar and thermoelectricity. Given the economic and sustainable factors concerning silicon, in addition to its role in relevant applications such as microelectronics and solar power. Silicon emerges as a natural selection to build our alloys around. Furthermore, the development and research on both high entropy alloys and metal silicides have been heavily centered around 3d transition metals. Keeping in line with the economic and environmental factors, we will continue this direction by focusing on high entropy stabilized sustainable and economic 3d metal silicides **Not happy with this writing**. Throughout the study we will analyze a great number of permutations of 3d silicides, from different initial metal silicides such as  $CrSi_2$ ,  $FeSi_2$ ,  $MnSi_{1.75}$ ,  $Fe_2Si$ , each with distinct properties relating to the band gap, crystal structure and metal to silicon ratio. In addition, the permutations include numerous metal distributions and elements within the 3d-group of metals. Examples are Co, Cr, Fe, Mn, and Ni.

Given a background in high-entropy alloys, one could ask if this study is truly sensible. In the later sections we will cover the details of this field, and it quickly become clear that the materials investigated in this study does not fall under the precise definition of high-entropy alloys, nor do we intend to explore the properties and factors relating to high-entropy stabilized alloys such as the configurational entropy, phase stability and finite temperature studies. However this study is motivated from the discovery of these materials and promising properties, and venture into a more hypothetical space of materials, enabled by the computational methods available to study the potential properties of such materials. On the other hand, very recent studies **Mari, and other HEA silicide study** have experimentally produced high-entropy disilicides, thus in some way justify the orientation of this project.

We begin this project by reviewing key concepts of solid-state physics for readers lacking a background in materials science, and an introduction to the base 3d silicides of the experimental work. Later follows a theoretic walk-through of the relevant concepts of this thesis, these topics include high-entropy alloys, special quasi-random structures, and density functional theory. Next we shine light on the implementation of DFT in this project, and other computational details required to reproduce the results in this thesis, such as the use of the Vienna Ab Initio Simulation Package (VASP) and implementation of SQS. Finally we present the results of our study, these include the band gap and electronic properties of various structures and the success and challenges of the computational methods applied throughout the study.

# **Part I**

# **Theory**

## Chapter 2

# Background

References: "Introduction to Solid-State physics", "Understanding solids", "Solid-state electronic devices", databases

### 2.1 Overview of solid-state physics

- Crystal structure
- Reciprocal lattice + Brilluin zone
- Chemical bonding + orbitals + energy bands
- Band gap + DOS ++

### 2.2 3d Silicides

In this project, we will build high-entropy silicides based on several promising 3d silicides, in terms of particularly the band gap. The silicides are  $CrSi_2$ ,  $MnSi_{1.75}$ ,  $FeSi_2$  and  $Fe_2Si$ . A summary of their most relevant properties for this project is listed in table .., and their corresponding crystal structure is displayed in figure ..

More information on these here...

## Chapter 3

# High-Entropy alloys

To begin this project, we give a brief description of high-entropy alloys (HEA). We introduce the basics and definitions, as well some more advanced topics relating to the functional properties of HEA's. This section will be largely based on the fantastic description of HEA's in "High-Entropy Alloys - Fundamentals and Application" [1] and the references therein, it's an excellent read.

### 3.1 Fundamentals

High-Entropy Alloys are a quickly emerging field in materials science due to the infinitely many possibilities and the unique properties. From the original discovery by Jin in 2004, as of 2015 there have been over 1000 published journal articles on high-entropy alloys. In its simplicity, a high-entropy alloy can be compared to a smoothie. By combining an assortment of fresh fruit and vegetables one can produce unique combinations of flavors and nutritional values based on both the properties of the distinct items, and their interplay in the mixture. In materials science, this exact procedure can be applied to generate a large range of materials with tunable properties depending on the intended application. In the topic of HEA's, this can be increased strength or ductility, corrosive resistance or lowered thermal conductivity, all of which have been observed in actual high-entropy alloys. Moving on from the rather banal fruit analogy, a high-entropy alloy typically falls under the two conditions.

1. The material consist of at least 5 distinct elements, where each element contribute between 5-35% of the composition
2. The total configurational entropy is greater than  $1.5R$ , where  $R$  is the gas constant.

The latter is an especial case for high-entropy alloys. The ideal configurational entropy of random  $N$ -component solid-solution is given in eq 3.1

$$\Delta S_{\text{config}} = -R \sum_{i=1}^N X_i \ln X_i, \quad (3.1)$$

it's clear that  $\Delta S_{\text{config}}$  increase with a higher number of constituents in the mix. For instance, the ideal configurational entropy of a binary alloy is  $0.69R$ , while a 5-component alloy is  $1.61R$ . If we neglect other factors that influence the formation of solid solutions (will be covered later), from Gibbs free energy in eq 3.2

$$\Delta G_{\text{mix}} = \Delta H_{\text{mix}} - T\Delta S_{\text{mix}}, \quad (3.2)$$

the two primary factors in formation of solid solution is the mixing enthalpy, which is the driving force to form compounds, and the mixing entropy which is the driving force to form random solid solutions. At elevated temperatures especially, the energy associated to the entropy of the system becomes comparative to the mixing enthalpy and can impact the overall equation. In summary, the overall concept of high-entropy alloys is that through alloying a greater number of elements, the gain in configurational entropy of the system prohibit the formation of intermetallic compounds in favor of a random solid solution. The random term simply relate to the various components occupying lattice positions based on probability. In fact, a narrower definition of high-entropy alloys would be structures with a single-phase disordered solid solution. The two "definitions" given previously can be considered as guidelines for the latter.

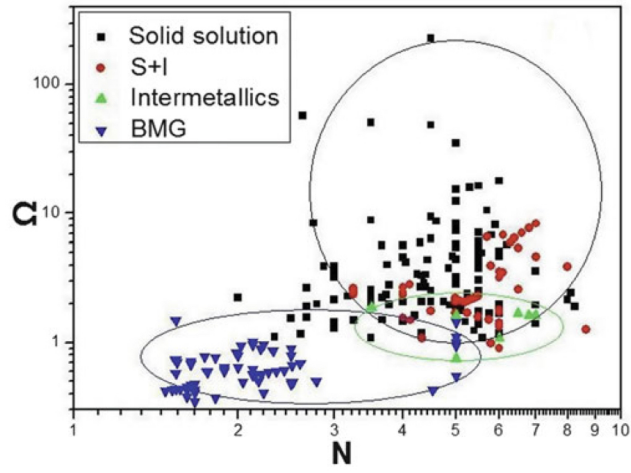
All though the mixing entropy mentioned above plays a central role in the formation, there are other factors to consider, and some that may oppose the formation of a single disordered phase. One of these is the atomic size effect which is related to the differences in atomic size, between the various elements in the alloy, this quantity is denoted  $\delta$ . Y. Zhang et al. in 2008 illustrated the relationship between  $\Delta H_{\text{mix}}$  and  $\delta$ . When  $\delta$  is very small, ie similar atomic sizes. The elements have an equal probability to occupy lattice sites to form solid solutions, but the mixing enthalpy is not negative enough to promote formation of solid solution. Increasing  $\delta$  does result in greater  $\Delta H_{\text{mix}}$ , but leads to a higher degree of ordering. **Include figure?** To summarize the illustration, the formation of solid solution high-entropy alloys occur in a narrow range of  $\delta$  value that satisfy both the enthalpy of mixing and the disordered state. Recently, Yang and Zhang proposed the parameter  $\Omega$  to evaluate the stability of high-entropy alloys. The quantity is a product of the melting temperature  $T_m$ , mixing entropy and mixing enthalpy in the following manner

$$\Omega = \frac{T_m \delta S_{\text{mix}}}{|\Delta H_{\text{mix}}|}. \quad (3.3)$$

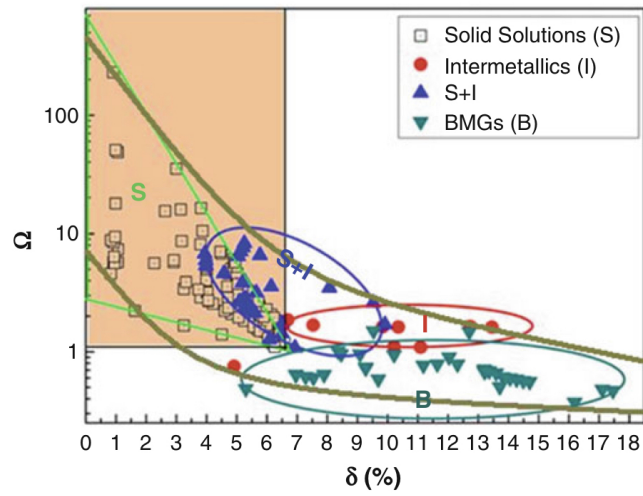
. They managed to obtain a qualitative condition for formation of the single disordered solid solution at  $\Omega \geq 1.1$  and  $\delta \leq 6.6\%$ . While compounds such as intermetallics form for greater values of  $\delta$  and lesser values of  $\Omega$ . Similarly, replacing the atomic size effect constant for the number of elements result in an equivalent condition. The results are summarized in figure 3.1

An important quantity in terms of characterizing high-entropy alloys is the total number of electrons VEC. The valence electron concentration of





(a) HEA formation based on  $\Omega$  and  $\delta$



(b) HEA formation based on  $\Omega$  and  $N$

Figure 3.1: Formation of HEA based on  $\delta$  and  $N$ . Figures adopted from [1]

a material is strongly related to the crystal structure of the material. For example,  $Co_3V$ , originally a hexagonal structure can be transformed into a tetragonal or cubic structure by either increasing the VEC from alloying with Ni, or reduction with Fe respectfully. Derived from the work of Guo et al. on the phase stability of a  $Al_xCrCuFeNi_2$  HEA, the VEC can be directly related to the crystal structure of high-entropy alloys. A lower VEC stabilize the BCC phase, while higher values stabilize FCC. In between is a mixture of the two. Specifically values greater than 8.0 stabilize FCC, and values below 6.87 favor BCC. However, these boundaries are not rigid when including elements outside of transition metals, exceptions have also been found for high-entropy alloys containing Mn. All though a heavy majority of reported high-entropy alloys that form solid solutions have been found to adopt simple cubic structures such as FCC and BCC. Recent studies have observed HEA's in orthorhombic structures like  $Ti_{35}Zr_{27.5}Hf_{27.5}Ta_5Nb_5$  and hcp structures, for example  $CoFeNiTi$ .

### 3.2 Core effects and properties of high-entropy alloys

Next, we will summarize the discussion above into four core elements that distinctly describe high-entropy alloys and their implications on the functional properties. The first of these is the "high-entropy effect", as the name suggests this is related to the increased configurational entropy from the amount of elements, that can inhibit the formation of strongly ordered structures. The second effect is the "severe lattice distortion effect", that originates from the fact that every element in a high-entropy structure is surrounded by non-homogeneous elements, thus leading to severe lattice strain and stress. The overall lattice distortion is additionally attributed to the differences in atomic size, bonding energies and crystal structure tendencies between the components. Therefore the total lattice distortion observed in HEA's are significantly greater than that of conventional alloys. This effect mostly affects the strength and conductivity of the material, such that a higher degree of distortion yields greater strength and greatly reduces the electronic and thermal conductivity due to increased electron and phonon scattering. An upside to this is that the scattering and following properties become less temperature dependent given that it originates from the lattice rather than thermal vibrations.

The two remaining effects, "sluggish diffusion" and "cocktail effect" can be summarized swiftly. The first is a direct consequence of the multi-component layout of high-entropy alloys that result in slowed diffusion and phase transformation because of the number of different elements that is demanded in the process. The most notable product from this effect is an increased creep resistance. Lastly we have the cocktail effect, which is identical to the smoothie analogy mentioned previously, in that the resultant characteristics is a combination of both the elements and their interaction. This is possibly the most promising concept behind high-entropy alloys, which fuels researchers with ambition to discover highly optimized materials by meticulously combining and predicting

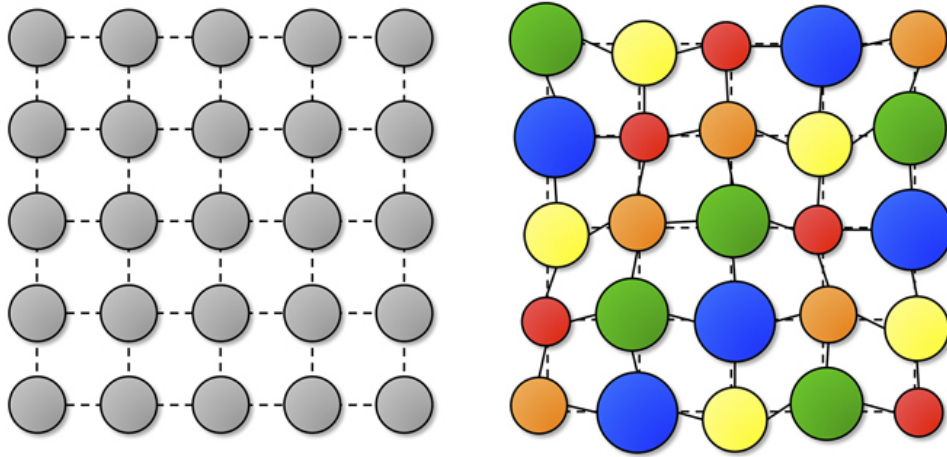


Figure 3.2: A schematic illustration of lattice distortion in high-entropy alloys. Figure from [2]

properties from different elements. Examples of this can be the refractory HEA's developed by "Air Force Research Laboratory" severely exceeding the melting points and strength of previous Ni or Co-based superalloys by alloying specifically refractory elements such as Mo, Nb and W. Another example is the research conducted by Zhang et al. on the high-entropy system  $FeCoNi(AlSi_{0-0.8})$  in the intent of unveiling the optimal combination of magnetic, electric and mechanical properties, resulting in an excellent soft magnet.

In the discussion above, we have covered the four core effects that make up high-entropy alloys and their relation to the mechanical and functional properties. Of the core effects, especially the lattice distortion and cocktail effect relate to the functional properties. The initial study on the functional properties on high-entropy alloys was conducted on the H-x alloy, referring to the system  $Al_xCoCrFeNi$  with  $0 \leq x \leq 2$ . It was found that the electrical resistivity was higher than that of conventional alloys, and that the conductivity generally decreased with increasing amounts of Al, additionally noteworthy low carrier mobility. Similar findings have also been made for the high-entropy alloy  $FeCoNi(AlSi)_x$ .

**Write a small part on magnetic and relate to the cocktail effect, then very briefly conclude by mentioning findings of superconductivity, corrosion resistance, hydrogen storage and other properties/applications.**

## Chapter 4

# Special quasi-random Structures

There are numerous difficulties involved with modeling of high-entropy alloys, or more general multi-component random alloys. **These are ...** Today, the most popular approaches are the coherent potential approximation (CPA), the virtual crystal approximation (VCA), the cluster expansion method, and special quasi-random structure (SQS). For this project, we exclusively used the latter primarily for it's direct and easy VASP implementation. Compared to the other approaches mentioned above, SQS reliably outperforms MC/MD simulations in terms of DOS calculations, and are significantly easier to implement and interpret. All though especially CPA is considered superior in simulating the electronic character of random alloys, combination with VASP is cumbersome and thus we opted for SQS as the building block of this thesis. **More on this? Cite relevant references on this, and restructure the paragraph to include more specif information and sources.**

### 4.1 The concept and fundamentals of SQS - Write proper later

Before the arrival of SQS and CPA methods, the common approach of modeling random alloys was to distribute the numerous elements randomly over the lattice sites. This was a costly operation, which either involved averaging a great number of possible configurations, or infeasible large supercells considering the computational efforts required. In the original paper on SQS published in 1990 [4] **Replace this article with the bigger SQS article from 1990**, it was proposed a selective occupation strategy (originally intended at random binary alloys) to design special periodic quasi-random structures that exceed previous methods in accuracy and cost. The key concept was to create a periodic unit cell of the various components in a finite  $N$  lattice site single configuration such that the structure most closely resemble the configuration average of an infinite perfect random alloy. In an attempt to work withing the

50 lattice sites boundary of ab initio methods at that time. The working theory was that if one can resemble an infinite perfect random alloy by a periodic finite N cell, also the electronic properties would be similar between the two. The solution to this model was that for each N, ie lattice site, to minimize the difference of structural correlation function between the approximated cell and the perfect random alloy. There are obviously errors involved with approximating a random alloy by a periodic cell, but by the hierarchical relation to the properties of the material, interactions between distant sites only offer a negligible small contribution to the total energy of the system. Thus the aim of the SQS method is focused around optimizing the correlations within the first few shells of a given site. To follow is a review of the mathematics related to the SQS method.

## 4.2 Mathematical formulation: Might need to expand on the definition and meaning behind terms such as clusters, figures, correlation functions etc (Add in post!)

Before describing the SQS approach, we begin by reviewing the concepts of topics such as cluster expansions, statistics and superposition of periodic structures. These topics are widely covered in the literature, we will simply focus on the summarizing the description given in [4]. Thus, we opt readers to refer to the original article or similar literature for a more comprehensive description of these topics. On a side note regarding the following mathematical derivation, the original concept was devolved for random binary alloys, but the theory have later been successfully extended to multi-component alloys as well.

The different possible atomic arrangements are denoted as "configurations"  $\sigma$ . The various physical properties of a given configuration is  $E(\sigma)$ , and  $\langle E \rangle$  is the ensemble average over all configurations  $\sigma$ . In practice, this quantity is unfeasible in terms of computational cost, seeing as the average require calculations and relaxations of all possible configurations, for a binary alloy this is  $2^N$  for a fixed N number of lattice sites. A solution to this is to use the theory of cluster expansions and discretize each configuration into "figures"  $f$ . A figure in the lattice is defined in terms of the number of atoms it include  $k$ , distance in terms of neighbors  $m$ , and position in the lattice  $l$ . Further we assign spin values for each lattice site  $i$  in the figure to denote which element it holds (+1,-1 for a binary alloy). By defining the spin product of spin variables in a figure at lattice position  $l$  as  $\Pi_f(l, \sigma)$ , we can write the average of all locations in the lattice of a given figure  $f$  as

$$\bar{\Pi}_f(\sigma) = \frac{1}{ND_f} \sum_l \Pi_f(l, \sigma) \quad (4.1)$$

where  $D_f$  is the number of equivalent figures  $f$  per site. The brilliance of this notation is that we now can express the physical property  $E(\sigma)$  in terms

of the individual contributions  $\epsilon_f$  of a figure  $f$ .

$$E(\sigma) = \sum_{f,l} \Pi_f(l, \sigma) \epsilon_f(l) \quad (4.2)$$

The quantity  $\epsilon_f$  is called the "effective cluster property" and is defined as (for a random binary alloy  $A_{1-x}B_x$ )

$$\epsilon_f(l) = 2^{-N} \sum_{\sigma}^{2^N} \Pi_f(l, \sigma) E(\sigma) \quad (4.3)$$

Inserting the equation for  $\vec{\Pi}_f$  into that of  $E(\sigma)$  we can describe the the previous cluster expansion of  $E(\sigma)$  as

$$E = N \sum_f D_f < \vec{P}_f > \epsilon_f \quad (4.4)$$

And obtain a simplified expression for  $< E(\sigma) >$  in eq 1? Thus we have successfully managed to reduce the expensive task of sampling all  $E(\sigma)$  into calculating the effective cluster properties and summing over all types of figures. Remembering that  $E(\sigma)$  can relate to many physical properties, the most common and applied case is that  $E(\sigma)$  is the total energy, while  $\epsilon_f$  is many body interaction energies. The cluster expansion above converge rather quickly with increasing number of figures, an effective method is thus to select a set of configurations to evaluate the effective cluster properties. Don't know how to write this, but the next step is to select a finite largest figure denoted  $F$ , and "specialize" the cluster expansion to a set of  $N_s$  periodic structures  $\sigma = s$  to obtain the two expressions for  $E(s)$  and  $\epsilon_f$  using matrix inversion to obtain the result for  $\epsilon_f$

$$E(s) = N \sum_f^F D_f \vec{\Pi}_f(s) \epsilon_f \quad (4.5)$$

$$\epsilon_f = \frac{1}{ND} \sum_s^{N_s} [\vec{\Pi}_f(s)] - 1E(s) \quad (4.6)$$

Assuming now that the sum of figures  $F$  and  $N_s$  periodic structures are well converged,  $E(\sigma)$  can be rewritten as a superposition of  $E(s)$

$$E(\sigma) = \sum_s^{N_s} \zeta_s(\sigma) E(s) \quad (4.7)$$

$$\zeta_s(\sigma) = \sum_f^F [\vec{\Pi}_f(s)]^{-1} \vec{\Pi}_f(\sigma) \quad (4.8)$$

where  $\zeta$  is the weights. Thus we have effectively reduced the problem to a convergence problem of the number of figures  $F$  and structures  $N_s$ . This can be easily solved given that we are dealing with periodic crystal structures  $s$  that can employ the general applications of ordered structures from ab initio methods, and increasing  $F$  until the truncation error falls

bellow a desired threshold. However, this approach requires that the variance of the observable property is much lower than the sample mean, otherwise one would have to employ a much bigger sample size to reach statistical convergence. Don't how to write this part nicely, but: Because of the different relationship between various physical properties and the correlation functions, one observe different convergence depending on the meaning of  $E$ . The idea behind SQS was therefore to design single special structures with correlation functions  $\vec{\Pi}_f(s)$  that most accurately match those of the ensemble average of a random alloy  $\langle \vec{\Pi}_f \rangle_R$ .

The correlation functions of an perfect random infinite alloy, denoted as  $R$  is defined bellow

$$\vec{\Pi}_{k,m}(R) = \langle \vec{\Pi}_{k,m} \rangle_R = (2x - 1)^l \quad (4.9)$$

with  $k, m$  defined as before and  $x$  being the composition ratio of the alloy. In the case of an eqvimolar alloy ( $x = \frac{1}{2}$ ), the functions equal 0 for all  $k$  except  $\langle \vec{\Pi}_{0,1} \rangle_R = 1$ . If we now randomly assign either atom A or B to every lattice site, for a sufficiently large value of  $N$ , the goal is then to create a single configuration that best match the random alloy. Keeping with the  $x = \frac{1}{2}$  case, the problem is now that even though the average correlation functions of a large set of these structures approaches zero, like for the random alloy. The variance of the average is nonzero meaning that a selected structure of the sample is prone to contain errors. The extent of these errors can be evaluated from the standard deviations

$$\nu_{k,m}(N) = | \langle \vec{\Pi}_{k,m}^2 \rangle - \langle \vec{\Pi}_{k,m} \rangle^2 |^{\frac{1}{2}} = (D_{k,m}N)^{-\frac{1}{2}} \quad (4.10)$$

Given the computational aspects, it's obvious that economical structures with small  $N$  are prone to large errors. In fact, in some cases these errors can result in correlation functions centering around 1, as opposed to 0 for a perfect random alloy.

I don't know how to write the prelude to this part! (see section IIIA in [4]). The degree to which a structure  $s$  fails to reproduce the property  $E$  of the ensemble-averaged property of the random alloy can be described by a hierarchy of figures, see eq .. bellow

$$\langle E \rangle - E(s) = \sum_{k,m}^l D_{k,m} [(2x - 1)^k - \vec{\Pi}_{k,m}(s)] \epsilon_{k,m} \quad (4.11)$$

, the prime is meant symbolize the absence of the value 0, 1 for  $k, m$ . The contribution from the figure property  $\epsilon$  reduces for larger figures. In general, for disordered systems, the physical property "E" at a given point  $R$  falls of exponentially as  $|R - R'|/L$ , where  $L$  is a characteristic length scale relating to the specific property. Using this, the approach of SQS is to specify a set of correlation functions that hierarchically mimic the correlation functions of the random alloy. Meaning that it prioritize the nearest neighbor interactions. With the set of functions decided on, the objective it finally to locate the structures that correspond to the selected structures.

Finished :) Write a final conclusion on this SQS derivation and motivate the incredibly bored reader for the coming sections.

### 4.3 Results and Advances in SQS and application to high-entropy alloys

A big part of this is related to the use of periodic crystal structures, that can employ standard ab initio methods; see article [4]. **Write later, Begin with results of original SQS proposed in 1990, move on to mcsqs and finally mcsqs for HEA and results in that field. For references see: see ch 10 book HEA, mcsqs article and later sections in [4]**

Following the 1990 paper, in 2013 a team of researchers further developed the concept of SQS to the current method used today, by the addition of monte-carlo algorithms [3]. **Write later**

Today SQS have been successfully applied to study formation energies, elastic properties, bond lengths, density of states, band gaps, plus more for a number of disordered structures, including semiconductors, metals, and high-entropy alloys. **Last section of 10.1, maybe include references from this section?** However, a large portion of SQS studies relate to binary and ternary alloys, with a very limited amount of literature on SQS on high-entropy alloys.



## Chapter 5

# Density-Functional Theory

### 5.1 Review of Quantum Mechanics

#### 5.1.1 The Shrödinger equation

The Schrödinger equation composed of the wavefunction  $\Psi(\vec{r}, t)$  and Hamiltonian  $\hat{H}(\vec{r}, t)$  where  $\vec{r}$  and  $t$  is the spatial position and time respectfully.

$$i\hbar \frac{\partial}{\partial t} \Psi(\vec{r}, t) = \hat{H}(\vec{r}, t) \Psi(\vec{r}, t) \quad (5.1)$$

The time-independent shrödinger equation for the eigenvalues  $E_k$  of the  $k$ -th eigenvalue  $\psi_k(\vec{r})$

$$\hat{H}\psi_k(\vec{r}) = E_k\psi_k(\vec{r}) \quad (5.2)$$

Extending to a system comprised of multiple particles, we have the many-particle Shrödinger equation, involving the many-body Hamiltonian. This quantity is composed of the kinetic energy of  $N_e$  electrons  $T_e$ , the interaction energy between electrons  $U_{ee}$ , the kinetic energy of  $N_n$  nuclei, the coulomb interaction between nuclei  $U_{nn}$ , and finally the attractive interaction between nuclei and electrons  $U_{en}$ . In the equation bellow for the may-body equation, we use the following symbols and notation:  $m_e$  = electron mass,  $m_n$  = nuclei mass,  $\epsilon_0$  = permittivity in vacuum,  $q$  = particle charge,  $\alpha$  = nuclei number,  $Z_\alpha$  = atom number of nuclei  $\alpha$ ,  $r$  = position of electron,  $R$  = position of nuclei.

$$\hat{H} = T_e + T_n + U_{ee} + U_{nn} + U_{en} \quad (5.3)$$

$$\begin{aligned} &= - \sum_{j=1}^{N_e} \frac{\hbar^2 \nabla_j^2}{2m_e} - \sum_{\alpha=1}^{N_n} \frac{\hbar^2 \nabla_\alpha^2}{2m_n} + \frac{1}{4\pi\epsilon_0} \sum_{j=1}^{N_e} \sum_{j' < j} \frac{q^2}{|r_j - r_{j'}|} \\ &+ \frac{1}{4\pi\epsilon_0} \sum_{\alpha=1}^{N_n} \sum_{\alpha' < \alpha} \frac{q^2 Z_\alpha Z_{\alpha'}}{|R_\alpha - R_{\alpha'}|} - \frac{1}{4\pi\epsilon_0} \sum_{j=1}^{N_e} \sum_{\alpha=1}^{N_n} \frac{q^2 Z_\alpha}{|r_j - R_\alpha|} \end{aligned} \quad (5.4)$$

### 5.1.2 Simplifications and approximations to solve the many-electron Shrödinger equation

#### Born-Oppenheimer

Challenges with solving many-particle Shrödinger equation is i) computationally expensive, ii) need to know how  $\Psi$  depends on single particle wavefunctions  $\psi_k$ . To solve this complex problem, we need approximations. Particularly Born-Oppenheimer and Harte-Fock approximations. The first makes the cleaver and reasonable assumption that since the electron mass is negligibly small in comparison to that of a nuclei, we can treat the nuclei as point charges, enabling us to divide the eigenfunction into a separate electronic and nuclear part, ie

$$\Psi_k^{en}(\vec{r}, \vec{R}) \approx \Psi_k(\vec{r}, \vec{R})\Theta_k(\vec{R}) \quad (5.5)$$

where we have written the complete wavefunction in terms of an electronic part  $\Psi_k(\vec{r}, \vec{R})$  and nuclear part  $\Theta_k(\vec{R})$ . The dependencies come from the fact that electrons can respond instantaneously to new positions of the nuclei, therefore the  $\vec{R}$  dependence. Writing this in terms of the Hamiltonian we get

$$(T_e + U_{ee} + U_{en}) \Psi_k(\vec{r}, \vec{R}) = E_k(\vec{R})\Psi_k(\vec{r}, \vec{R}) \quad (5.6)$$

$$(T_n + U_{nn} + E_k(\vec{R})) \Theta_k(\vec{R}) = E_k^{en}(\vec{R})\Theta_k(\vec{r}, \vec{R}). \quad (5.7)$$

The two sections are interrelated through the electronic energy eigenvalue  $E_k(\vec{R})$ . Furthermore, the left hand side of the nuclear part can be simplified to  $U_{nn} + E_k(\vec{R})$ , assuming that the kinetic energy of point charges is zero. This simplified expression for the nuclear left hand side is called for the potential energy surface (EPS).

#### Hartree-Fock

The next step in line is to find a wavefunction that can describe all electrons in a system. This was originally done by Hartree, which assumed that electrons can be described independently and suggested the ansatz for a two-electron wavefunction

$$\Psi_k(\vec{r}_1, \vec{r}_2) = A \cdot \psi_1(\vec{r}_1)\psi_2(\vec{r}_2), \quad (5.8)$$

where A is the normalization constant. However this approximation does not account for the fact that electrons are indistinguishable and hence does not obey the Pauli exclusion principle for fermions. This was overcome with the Hartree-Fock approximation that implement an anti-symmetric wavefunction. The full expression is given bellow

$$\Psi_k(\vec{r}_1, \vec{r}_2) = \frac{1}{\sqrt{2}} \left( \psi_1(\vec{r}_1)\psi_2(\vec{r}_2) - \psi_1(\vec{r}_2)\psi_2(\vec{r}_1) \right) \quad (5.9)$$

The Hartree-Fock (HF) approximation makes the electrons distinguishable and hence obey the Pauli exclusion principle, this means that the exchange energy is accounted for. On the other side, HF is not a complete description as it fails to model the electron correlations.

## The Variational principle

In materials science, the overarching concern is the ground-state properties of a system. This can be found efficiently and easy by what's known as the variational principle. This states that the energy of any trial wavefunction will always be higher than the ground-state energy  $E_0$ , ie

$$E_0 = \langle \psi_0 | H | \psi_0 \rangle \leq \langle \psi | H | \psi \rangle = E \quad (5.10)$$

This enable us to find the ground state energy and corresponding wavefunction by a minimization technique. Next, we will present the basics of the density functional theory for how these equations can be solved numerically and efficiently in order to study real materials and systems.

## 5.2 Fundamentals of Density-Functional Theory

The density functional theory was developed by Hohenberg and Kohn in 1964 and revolved around the fact that the ground-state density can be expressed in terms of the ground-state wavefunction. We have

$$n_0(r) = |\Psi_0(r)|^2, \quad (5.11)$$

furthermore the theorem states that all ground-state physical properties can be found as unique functionals of the ground-state density. The biggest upside of this, is that instead of trying to solve the many-body Schrödinger equation to obtain the ground-state wavefunction, we have reduced the computational complexity from  $3N_e$  to 3. Thus, the Hohenberg and Kohn density functional theory makes for a promising and effective method to obtain the ground-state properties of a system, given that the exact electron density functional is known. However, this is still 60 years later unknown.

The density functional theory build on two specific theories, called the Hohenberg-Kohn theorems. They are:

1. For any system of interacting particles in an external potential  $V_{ext}$ , the density is uniquely determined.
2. There exists a variational principle for the energy density functional such that, if  $n$  is not the electron density of the ground-state, then  $E[n_0] < E[n]$ .

The proof behind both theorems can be found in appendix .. A direct result of the second theorem is the energy can be described as a function of the density

$$E[n] = T[n] + U_{ee}[n] + U_{en}[n], \quad (5.12)$$

where the first two terms  $T[n]$  and  $U_{ee}[n]$  make up the Hohenberg-Kohn functional.

We now move on to the Kohn-Sham equations, in which Kohn and Sham expressed the exact ground-state density from Hartree type wavefunctions.

$$\Psi(\vec{r}_1, \vec{r}_2, \dots, \vec{r}_{N_e}) = \psi_1^{KS}(\vec{r}_1) \psi_2^{KS}(\vec{r}_2) \dots \psi_{N_e}^{KS}(\vec{r}_{N_e}) \quad (5.13)$$

In which,  $\psi_j^{KS}$  are auxiliary independent single-particle wavefunctions. We now modify the equation for total energy as a function of density defined by the second theorem, to include the single auxiliary wavefunctions and their corresponding kinetic energy and interaction energy. We get:

$$E[n] = T_s[n] + U_s[n] + U_{en}[n] + (T[n] - T_s[n]) + (U_{ee}[n] - U_s[n]). \quad (5.14)$$

with the  $s$  subscript denoting the single particle wavefunctions. The latter two terms are known as the exchange-correlation energy  $E_{xc}$

$$E_{xc}[n] = \Delta T + \Delta U \quad (5.15)$$

This term is responsible for the many-electron interaction. The complete total energy functional can now be expressed as

$$\begin{aligned} E[n] = & \underbrace{\sum_j \int \psi_j^{KS*} \frac{-\hbar^2 \nabla^2}{2m} \psi_j^{KS} d\vec{r}}_{T_s[n]} + \underbrace{\frac{1}{2} \frac{1}{4\pi\epsilon_0} \int \int q^2 \frac{n(\vec{r})n(\vec{r}')}{|\vec{r} - \vec{r}'|} d\vec{r}d\vec{r}'}_{U_s[n]} \\ & + \underbrace{\int V_{en}(\vec{r})n(\vec{r})d\vec{r}}_{U_{en}[n]} + \underbrace{(T[n] - T_s[n]) + (U_{ee}[n] - U_s[n])}_{E_{xc}[n]} \end{aligned} \quad (5.16)$$

Finally we write the complete expression for the Kohn-Sham single-electron equations given an exact exchange-correlation energy and utilizing the variational principle described previously

$$\left\{ -\frac{\hbar^2}{2m_e} \nabla_s^2 + v_H(\vec{r}) + V_{en}(\vec{r}) + V_{xc}(\vec{r}) \right\} \psi_s^{KS}(\vec{r}) = \epsilon_s^{KS}(\vec{r}) \psi_s^{KS}(\vec{r}), \quad (5.17)$$

Define  $V_H$  and  $V_{xc}$  and mention that the former include self interaction that can be accounted for in XC functional. Finally, the total energy of the many-electron system is defined as

$$E[n] = \sum_j \epsilon_j^{KS} - \frac{1}{2} \frac{1}{4\pi\epsilon_0} \int \int q^2 \frac{n(\vec{r})n(\vec{r}')}{|\vec{r} - \vec{r}'|} d\vec{r}d\vec{r}' + E_{xc}[n] - \int V_{xc}(\vec{r})n(\vec{r})d\vec{r}. \quad (5.18)$$

This is the fundamental working principle of the density functional theory and Kohn-Sham equations.

### 5.3 The exchange-correlation energy

**Add references and other fixes later** If we can find an expression for  $E_{xc}[n]$  as a functional of the density, we have all the tools required to calculate

the total energy of any material. Given that the physical properties of a material is strongly related to the electronic density of said material, the precision of DFT is very dependent on the type of approximation to the density is used. However there exist a compromise here, as a more precise density model is significantly more complex and costly from a computational perspective. In this section we will discuss the extensions of DFT since the original formulation in 1960, and the different approximations one can apply to the electronic density. Thereafter we will discuss the application of DFT, therein the pros and cons, successes and failures.

The exchange-correlation functional is only exactly known for a homogeneous electron gas, however this is of limited use in real materials with a high degree of variation in the electron concentration. An improvement on this is the local density approximation (LDA), in which the electronic density is set at each position according to the homogeneous electron gas at that position, ie

$$V_{xc}(\vec{r}) = V_{xc}^{\text{gas}}[n(\vec{r})] \quad (5.19)$$

This is seen as a successful approximation for the exchange-correlation energy in bulk materials, given that typically the electron density does not vary tremendously. However this method is not without flaws, most notably is the presence/degree of self-interaction induced from this method, from that the self-interaction term does not completely cancel out by only including the local environment of given positions. This may lead to artificial contributions to  $V_{xc}$  and an overall inaccurately high electron density. The success behind this method most reliably lies in the low computational cost.

The generalized gradient approximation (GGA) extends on the concept of LDA by also including the gradient of the electron density.

$$V_{xc}^{\text{GGA}}(\vec{r}) = V_{xc}[n(\vec{r}), \nabla n(\vec{r})]. \quad (5.20)$$

GGA is good for materials with a slowly varying density, but fails with large gradients. The GGA functional is implemented in two different methods, Perdew-Wang 91 (PW91) and Perdew-Burke-Ernzerhof (PBE).

Both methods underestimate the band gap and wrongly predict the charge localization in cases of narrow bands or lattice distortion. A large part of this comes from the self-interaction of the Hartree potential. By combining the correlations and exchange of LDA/GGA with the exact exchange of the Hartree-Fock approximation, we can obtain much more precise calculations. This method was proposed by Becke and proposed as hybrid functionals, since the functional is a hybrid between the two. This method is superior in describing localized states, but comes at a significant larger computational cost. In order to reduce this cost, Heyd al et. split the Hartree-Fock exchange into short-range and long-range parts, in which calculations can adapt exact Hartree-Fock exchange for short-range (SL) and non-exact for long-range (LR). By introducing the parameter  $\omega$  to

adjust the order parameter of the method, we can express this method, called HSE (Heyd-Scuseria-Ernzerhof) by

$$E_{xc}^{HSE} = \alpha E_x^{HF,SR}(\omega) + (1 - \alpha) E_x^{PBE,SR}(\omega) + E_x^{PBE,LR}(\omega) + E_c^{PBE} \quad (5.21)$$

- Explain what the different notations mean, and the success + limitations of HSE compared to LDA and GGA.
- Write a paragraph on meta-GGA, such as SCAN and perhaps MBJ.

## 5.4 Success and limitation of DFT

- Local minima method
- Not exact  $V_{xc}$ , means we must compromise between accuracy and cost, and choose between the different methods for specific application. There is no one best overall method that is superior for all purposes.

**Part II**

**Methodology and  
Implementation**

## Chapter 6

# Practical application of DFT

In this section we will present how the density functional theory discussed above can be applied and implemented in a computationally feasible manner to model various materials.

**Insert section in XC functionals here.** With the exchange-correlation functionals presented above, we now have everything in order to perform DFT calculations. To begin solving eq .., we need the single-electron wavefunction, for a free electron this is a plane wave  $\psi_k = Ae^{ikr}$ . In a solid however, there exist a nonzero periodic potential  $V(\mathbf{r}) = V(\mathbf{r} + \mathbf{R})$ , the solution to the Shrödinger equation is given by Bloch's theorem wich states that the solution takes the form

$$\psi_k(\mathbf{r}) = u_k(\mathbf{r})e^{ikr}, \quad (6.1)$$

where  $u_k(\mathbf{r})$  is a bloch wave with identical periodicity to the supercell. And  $k$  is the wavevector. Along with eq(above), problems in DFT are solved in  $k$ -space or reciprocal space for convience sake. For instance a great deal of DFT calculations revolve around solving the integral

$$g = \frac{V_{\text{cell}}}{(2\pi)^3} \int_{\text{BZ}} g(\mathbf{k}) d\mathbf{k}, \quad (6.2)$$

with BZ denoting that the integral be evaluated for all  $k$  in the Brillouin zone. This integral can be approximated by evaluating the integral at a set of discrete points and summing over the points with appropriately assigned weigts. A larger set of points leads to more exact approximations. This method is called Legendre quadrature. The method for selceting these points in reciprocal space was devolped by Monkhorst and Pack in 1976, and simply put requieres a amount of kpoints in each direction in reciprocal space, in the form  $N_x N_y N_z$ . Recalling that reciprocal space is inverse to regular space, supercells with equal and large dimensions converge at smaller values of N, and inversly for cells of small dimnsion. In supercells with different length axis, such as hexagonal cells, we use the notation  $N_x N_y M$ , where  $M$  relate to the distincntly different axis. The amount of kpoints required can be fruther reduced by utulizing the symmetry of the cell, in which we can exactly approximate the entire BZ by extending a



lesser zone through symmertry. This reduced zone is appropriately named the irreducible Brillouin zone (IBZ).

Metals in particular requiere a large set of kpoints to acchive accurate results. This is becuse we encounter discontinuies functions in the Brillouin zone around the fermi suface where the states discontinusly change from occupied to non-occupied. To reduce the cost of this operatin, there are two primary methods, tetrhaedon and smearing. The idea behind the tetrahedon method is to use the discrete set of k-points to fill the reciprocal space with tethraeda and interpolate the function within each tethraeda such that the function can be integrated in the entire space rather than at discrete points. The latter approach for solving discontinuos integrals is to smear out the discontinuity and thus transforming the integral to a continous one. A good analogy to this method is the fermi-dirac function, in which a small variable  $\sigma$  transform a step-functino into a continious function that can be integrated by standard methods.

In addition to the number of kpoints, there is one more distinct parameter that must be specified in DFT calculations, namely the energy cutoff, or  $E_{\text{cut}}$ . This parameters arise from the Bloch function described previosly. In which  $u_k(\mathbf{r})$  was a bloch wave with the same periodicity as the supercell. This implies that the wave can be expanded by a set of special plane waves as

$$u_k(\mathbf{r}) = \sum_{\mathbf{G}} c_{\mathbf{G}} e^{i\mathbf{G}\mathbf{r}}, \quad (6.3)$$

where  $\mathbf{G}$  is the reciprocal lattice vector. Combining this with eq ..(first eq for blcoh function) we get

$$\psi_k(\mathbf{r}) = \sum_{\mathbf{G}} c_{\mathbf{k}+\mathbf{G}} e^{i(\mathbf{k}+\mathbf{G})\mathbf{r}} \quad (6.4)$$

The consequense from this expression is that evaluating the wavefunction of an electron at a single  $k$  point demand a summation over the entirity of reciprocal space. In order to reduce this computational burden, we can introduce a maximum paramater  $E_{\text{cut}}$  to cap the calculations. This is possible becuse eq ..(above) is the solution of the Shrödinger equation with kinetic energy

$$E = \frac{\hbar^2}{2m} |\mathbf{k} + \mathbf{G}|^2. \quad (6.5)$$

Seeing as the solution with lower energies are the most interesting, we can limit the calculations of eq ..(2 above) to solutions with energy less than  $E_{\text{cut}}$  given bellow

$$E_{\text{cut}} = \frac{\hbar^2}{2m} G_{\text{cut}}^2. \quad (6.6)$$

Thus, we can reduce the infinitely large sum above to a much more feasable calculation in

$$\psi_k(\mathbf{r}) = \sum_{|\mathbf{k}+\mathbf{G}| < G_{\text{cut}}} c_{\mathbf{k}+\mathbf{G}} e^{i(\mathbf{k}+\mathbf{G})\mathbf{r}} \quad (6.7)$$

**A summary on kpoints and ENCUT, plus a discussion on nummerical convergence and how to select kpoints and ENCUT**

A final consideration to how DFT is applied in practise is how the core electrons are handled. Tightly bound core electrons as opposed to valence electrons demand a greater number of plane-waves to converge. The most efficient method of reducing the expenses of core-electrons are so-called pseudopotentials. This method works by approximating the electron density of the core electrons by a constant density that mimic the properties of true ion core and core electrons. This density is then remained constant for all subsequent calculations, ie only considering the valence electrons while regarding the core electrons as frozen-in. There are currently two popular types of pseudopotentials used in DFT, so-called ultrasoft pseudopotentials (USPPs) developed by Vanderbilt, and the projector augmented-wave (PAW) method by Bloch. This project will exclusively apply the latter.

#### **Self-consistent iteration and relaxation discussion and figure**

## Chapter 7

# Computational details

This section is intended to provide the necessary details for reproduction of results to be presented later on. First we begin by describing the software used for the project.

### 7.1 Vienna Ab initio Simulation Package

This software, often referred to as VASP is a package for ab initio quantum mechanics calculations using the projected augmented wave method and plane wave basis set. The intended methodology is DFT, but have been extended for methods post the original DFT-formulation. Calculations with VASP was carried out on the supercomputer fram, with allocated time and resources provided by Uninett Sigma2,**add reference!**

The structure of VASP rely on a set of input files and output files from the calculation, the input files required to perform a DFT computation in VASP are the following:

- INCAR - this file provide the tags responsible for different methods, algorithms, parameters etc.
- POSCAR - this file is related to the crystal structure of the system
- POTCAR - What psudopotential that is used
- KPOINTS - A file containing information on what KPOINTS will be used
- jobfile - This file contains information for the supercomputer regarding resources and such.

The capitalization displayed above is directly related to the requirements of the file system in the VASP/fram collaboration. Some important output files are:

- CONTCAR - The relaxed crystal structure after finalized calculation
- CHGCAR - This file contains the electron density after calculation

- EIGENVAL - Contains the solutions to the Kohn-Sham eigenfunctions
- DOSCAR - Information on the Density of States
- OUTCAR - Contains a list of all other information.

In this project, we began the calculation of every individual structure by testing the convergence of total energy with respect to the number of k-points and cutoff energy. In VASP, the latter can be specified by setting the tag "ENCUT" in the INCAR file, we found 300 eV to yield productive results in terms of convergence and computation time for total energy calculations, and 400 for ionic+volume relaxations. Regarding the number of points in the reciprocal space, we carried out a great deal of simulations on numerous structures with distinct crystal structures and corresponding supercells, for this reason we employed a number of different sets of k-points depending on the structure. Typically the number of points ranged from a 2x2x2 mesh to 4x4x4 mesh. With the smaller being required for hybrid functionals to converge.

Upon realizing the convergence parameters, the structures were allowed to relax both the ionic positions, and cell volume with the quasi-newton method and a convergence criterion of  $1E - 2$  for the forces and  $1E - 5$  for the total energy. However, the symmetry of the structure was forced constant by the use of vasp-std-noshear. This process was repeated two times before performing one final total energy calculation with GGA functional, and one with the SCAN functional, increasing the convergence criterion to  $1E - 6$ . In certain cases, we also attempted to perform calculations with the hybrid functional HSE06.

The specific tags, algorithms, parameters and options of VASP that was in use throughout this project can be found at our GitHub address, but in particular we would like to cover specifically two factors/tags. Firstly is the tag ISPIN that correspond to the magnetism of the system. Considering this study revolved heavily around magnetic elements such as iron and Nickel, we used ISPIN=2 which allow for co-linear spin-polarized calculations. However, there are many more magnetic orientations the system can adopt besides co-linear, therefore the final total energies we found may not be the true lowest energies. But given the allocated duration and resources of this project, this is a understood consequence. Secondly is the type of smearing that was used for the different calculations. The preferred method for accurate total energies and density of states in semiconductors is the tetrahedron method, and for accurate forces in metals the Methfessel-Paxton method is recommended. However, our system contains both metals and a large portion of Si. For this reason we used a combination of smearing methods. For the relaxation and minimization of forces, we used gaussian smearing with smearing width  $\sigma = 0.05$ , as this method provide accurate forces in both metallic and semiconducting materials. And to calculate the total energy and DOS, we used the tetrahedron method, as recommended. One interesting result of this project, is that we were not able to converge calculations with hybrid functionals using the tetrahedron

method and was thus forced to adopt the Gaussian method in this case additionally.

**Band structure/DOS and band-unfolding?**

## 7.2 Generation of SQS

The generation of special quasi-random structures as described in section .., was done by utilizing the Temperature Dependent Effective Potential (TDEP) method. This package, devolved by Olle Hellman, offers a wide range of tools primary intended for studies of finite temperature lattice dynamics. In this project we utilize the program generate-structure within the TDEP package to construct SQS's. The work of TDEP is the result of an unpublished PHD thesis by Nina Shulumba (**Insert citation**), thus the documentation on the software and generate-structure script is limited, please refer to the original author for more information.

In this project, we constructed SQS's by first transforming the cif-files of a given initial structure, for instance that of  $FeSi_2$ , to a primitive unit cell. The SQS's was generated by the same principles explained in section .., for each structure we created 5 distinct SQS's of an equal size under the constraint that the 3d atoms be distributed eqvimolar in the system. Precise file formats and such can be found at GitHub. Another approach could have been to construct SQS's of specific cell counts instead of total number of atoms, however this quickly lead to extremely large supercells, up to 256 atoms, that simply would not converge to our best efforts.

We began by studying high-entropy silicides by alloying 3d-metal silicides such as  $Fe_2Si$  by Cr, Fe, Co, and Ni to construct a  $(CoCrFeNi)_2Si$  alloys. From this point we varied the distribution and type of elements in an attempt to locate high-entropy silicides with semiconducting properties.

**Insert figure of SQS's before relaxation, for some of the structures and give a brief summary.**

## 7.3 Utility scripts

During the course of the projects lifetime, several shell and python scripts was developed by myself and/or provided to me by my supervisor Ole Martin Løvvik and his team of researchers at Sintef. These can be located at the GitHub address :...

**Part III**

**Results and Discussion**

## Chapter 8

# Results of SQS

### 8.1 Something

Compare the results from different SQS in terms of stability and total energy: Factors to include can be bond length, nearest neighbors, density, structure, element, size of SQS, initial magnetic settings. ETC

## Chapter 9

# Band gap results

### 9.1 Compare and analyze band gaps

Results here can be a table of the band gaps for different SQS both within one cell, or compare multiple cells. Other results include Density of States, Local DOS, bandgap from eigenval without impurity states. Compare different methods, GGA, SCAN and hybrid. The CHGCAR to evaluate bonding in terms of metallic or covalent. Possibly band-unfolding?



**Part IV**

**Conclusion**

# Bibliography

- [1] Michael C Gao et al. *High-Entropy Alloys*. 1st ed. Springer, Cham, 2016. URL: <https://doi.org/10.1007/978-3-319-27013-5>.
- [2] Lewis Robert Owen and Nicholas Gwilym Jones. 'Lattice distortions in high-entropy alloys'. In: *Journal of Materials Research* 33.19 (2018), pp. 2954–2969. DOI: 10.1557/jmr.2018.322.
- [3] A. van de Walle et al. 'Efficient stochastic generation of special quasirandom structures'. In: *Calphad* 42 (2013), pp. 13–18. ISSN: 0364-5916. DOI: <https://doi.org/10.1016/j.calphad.2013.06.006>. URL: <https://www.sciencedirect.com/science/article/pii/S0364591613000540>.
- [4] S.-H. Wei et al. 'Electronic properties of random alloys: Special quasirandom structures'. In: *Phys. Rev. B* 42 (15 Nov. 1990), pp. 9622–9649. DOI: 10.1103/PhysRevB.42.9622. URL: <https://link.aps.org/doi/10.1103/PhysRevB.42.9622>.